Test facility development for the SPICA-SAFARI instrument

Pieter Dieleman, Bart Vandenbussche, Bruce M. Swinyard, Willem Jellema, Marc Ferlet,
Lenze Meinsma, Wouter M. Laauwen, Lorenza Ferrari, Heino Smit, and Martin Eggens

Abstract— **In this article the main characteristics of the SAFARI instrument onboard SPICA are described, as well as a proposed setup to verify function and performance of the instrument. A major challenge is the required low background light level, which excludes the use of cryostat windows and hence all test sources need to be inside the cryostat. The maximum allowed temperature for any unit inside the 4K compartment is 8K to minimize heat radiation affecting the detector NEP. A concept for a calibration source is introduced which operates up to 200 K with an attenuation factor of 10^6. A beam quality test method is proposed as well. Finally, a total system concept is presented.**

Index Terms— **Submillimeter wave receivers, infrared spectroscopy, system testing, submillimeter wave measurements, cryogenics.**

I. INTRODUCTION

S AFARI (SpicA Far-infraRed Instrument) is an imaging Fourier Transform Spectrometer with a 2'x2' instantaneous field of view (FoV) for the 34 – 210 µm wavelength region. The architectural design of the instrument is similar to that of the Herschel/SPIRE instrument [1],[2]. The instrument is being developed by a European consortium led by SRON, the Netherlands Institute for Space Research. It is scheduled for launch in 2018 onboard the SPace Infrared telescope for Cosmology and Astrophysics (SPICA) satellite, developed jointly by JAXA and ESA. The main advantage of SPICA over Herschel is its actively cooled mirror, allowing orders of magnitude more sensitive detectors to be used. SAFARI offers imaging spectroscopy and imaging photometry in the far infrared with detector NEP of $2 \cdot 10^{-19}$ W/√Hz and a spectral resolution of R = $\sigma/\Delta\sigma$ = 2000. To reach this sensitivity the SAFARI instrument uses TES (Transition Edge Sensor) detectors[3] operated at 50 mK. This temperature is reached by a combination of a sorption cooler and ADR inside the Focal Plane Unit (FPU). The FPU, including the optics and mechanisms, is cooled to 4.5K. The SAFARI wavelength range is split into 3 bands: 34 – 60, 60 – 110, and 110 – 210 µm. To allow for direct sky mapping without jiggling, Nyquist sampling of the FoV is required, leading to a total number of pixels of about 4000. Efficient readout is obtained by Frequency Division Multiplexing (FDM), using 1 SQUID amplifier per channel consisting of 160 pixels.

In this article we describe the considerations in designing a cryogenic test facility for SAFARI on-ground calibration and characterization. A major challenge will be to meet the required low background (a few attoWatts per pixel) whilst providing the SAFARI Focal Plane Unit with the necessary calibration sources. The layout of this article is as follows: in section 2 the tests to be performed are described as well as the requirements for the Optical Ground Support Equipment (OGSE), the test equipment inside the cryostat. Section 3 describes the optical design of the OGSE as well as the status of the design of the various OGSE elements. Section 4 will go in on the status and development approach of light tightness measures.

II. SAFARI GROUND TESTS

The characterization of a sensitive imaging spectrometer primarily focuses on the following aspects: Radiometry - to measure the sensitivity of the detectors and calibrate the calibration source internal to the instrument, Image quality – to measure the corresponding sky position of each pixel, Frequency resolution and frequency accuracy – to calibrate the spectrometer function of SAFARI. Critical issues specific for SAFARI are thermal and EMC compatibility of the TES detector system with the ADR cooler and FPU mechanisms. The critical SPICA interfaces with SAFARI are mechanical, thermal, electrical and optical: High launch loads of 20g sine, microphonics[4], temperature stability and cooling power, EMC and stray light. The AIV (Assembly Integration and Verification) program aims at an early optimization and verification of these critical items. The tests required and resulting hardware are presented in Table 1. Since these aspects require both development and qualification, a 3-model philosophy is chosen: A Demonstration model (DM) to show

P.Dieleman, W. Jellema, L. Meinsma, W.M. Laauwen, L. Ferrari, H. Smit, M. Eggens are with the SRON Netherlands Institute for Space Research, Landleven 12, 9700 AV Groningen, the Netherlands (Phone: +31503638286, email: P.Dieleman@sron.nl).

B. Vandenbussche is with the Institute of Astronomy K.U. Leuven, Celestijnenlaan 200B, 3001 Leuven, Belgium.

B.M. Swinyard and M. Ferlet are with the Rutherford Appleton laboratory, Chilton, Didcot OX11 0QX, united Kingdom.

L. Meinsma is with Annex, Bellingeweer 16, 9951 AM Winsum, the Netherlands.

TABLE I
SAFARI TESTS AND RESULTING HARDWARE

Category	Test method	Test equipment
Image quality		
- Sky mapping	Point source scan in OFP[a]	Cryo XY stage, pinholes, broadband source
- Beam direction	Multiple scan planes	Z-axis in OFP scanner
- FTS wander	Scan FTS	Stable pinhole mask in OFP
- Pupil quality	Point scan in OPP[b]	X(Y) stage, pinhole in OPP
- Stray light	scan beyond OFP and OPP diameters	scan range 3 x plane size
- Cross talk	Point source mask in OFP	Representative reimager, pinhole masks
-		
Linearity		
- Continuum	Increasing background with chopped weak line	Instrument Flasher with calibration source + etalon
- Line	Line strength variation	Chopper external laser with power tuning (grid)
Radiometry		
- calibration	Test internal against external calibrator	OGSE calibration source
- flatness	Measure NEP, gain	OGSE flatfield source
- source size	Measure NEP versus point source size	Back-illuminated pinhole wheel
Spectrometry		
- frequency	Known line source, FTS scans	External laser, calibrated cryo etalon, gas cell
- resolution	Narrow line source, FTS scans	External laser
Stability		
- noise, gain	Measure stable line signal for tbd period	Internal calibration source with etalon

[a]OFP stands for Object Focal Plane, the reimaged focal plane of the SAFARI FPU. [b]OPP stands for Object Pupil Plane, the reimaged pupil plane internal to the SAFARI FPU.

that the planned performance will be achievable and to find functional issues, a Qualification Model (QM) to verify SAFARI will survive the launch and space environment, and the Flight Model (FM), to be launched after full verification.

III. OGSE DESCRIPTION

The equipment common for all tests are: A reimager with similar optical properties as the SPICA telescope, a pupil scanner, a calibration source in the reimaged focal plane (OFP), and a mask plate in the OFP back-illuminated by a wide-band and spectral source. Fig. 1 shows the OGSE assembly with all units mentioned in Table 1.

A. Reimager

The reimager consists of a flat folding mirror and 2 off-axis parabolas. The layout is similar to that of the PACS OGSE [5], although optimized for shorter wavelengths and lower geometric distortion by reducing the angles of incidence. Spot diagrams below indicate geometric spot size well below the Airy pattern size over the full FoV. The reimager used for the instrument level tests has a significantly smaller wavefront error than the SPICA telescope specification.

The magnification is determined by the limited size of a back-illuminating integrating sphere, and by the requirement
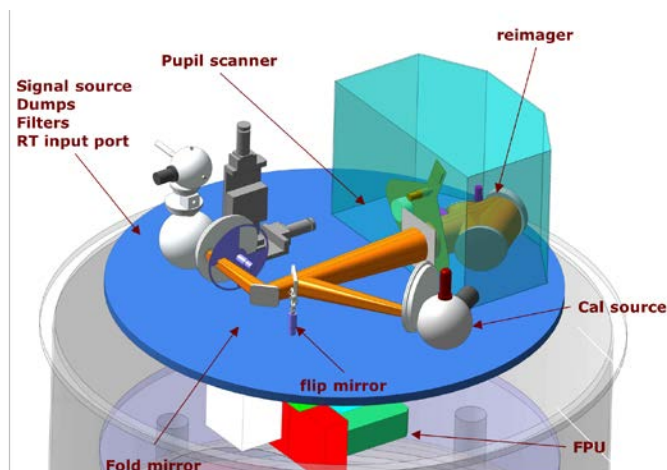

Fig. 1. OGSE layout inside the SAFARI test cryostat. The blue plate is the optical bench, the FPU is hanging upside-down at the lower side. The FPU beam goes through the optical bench, via a reimager into the OGSE space. The OGSE pupil stop acts as an additional stray light baffle, and at this position the pupil scanner is located. The beam is deflected by a flip mirror towards the cryogenic calibration source, or continues toward an XY scanner system with a pinhole mask wheel back-illuminated by an integrating sphere. This sphere is fed by an internal source directly, or via filters or etalons, and can be fed by a room temperature source via a light pipe as well. Both the FPU and OGSE will be enclosed by 4K light tight shield (not shown)

that the point source size must be larger than a wavelength for proper transmission while still be much smaller than the OFP Airy disk for accurate PSF scanning. The optimum lateral magnification is found to be 1.86, hence the 10x10 mm focal plane is reimaged on an 18.6x18.6 mm grid.

Similarly, the FPU pupil stop is reimaged in a plane in the OGSE space. In order to determine both position and direction of the FPU beam, the position of the reimaged beam on the OGSE pupil plane as well as field plane needs to be measured.

B. Pupil Plane beam measurement

The image of the FPU pupil in the OGSE has a diameter of 80 mm, the position of this plane is shown in Fig. 1 The f-number of the optics for this plane is 30, which gives an airy disk radius of 1.22 $F\cdot\lambda$ = 1.4 mm for the shortest SAFARI wavelength, hence an appropriate pinhole size is 1 mm. For stray light measurements the point source needs to move out of the plane by 40 mm in all directions, hence the total pupil diameter to be scanned is 160 mm.

C. Focal Plane beam measurement

The types of measurements performed with the FP scanner are pixel spatial response, focal plane geometry and stray light (ghosts). The purpose of spatial response measurements is to verify the image quality, field curvature, and image distortion. The focal plane geometry gives information about the number of the pixels and the pitch. The strategy is to scan the focal plane with a pinhole mask, back-illuminated by an integrating sphere [6]. The pinhole size differs for the different bands to keep the pinhole diameter larger than the wavelength which avoids spectral power differences, but significantly smaller than the pixel size. The focal plane is curved; the instrument optics maps a flat TES aperture plane to a curved image with a

radius of curvature of about 550 mm. During a final XY scan the scanner will follow in Z the curved focal plane.

The source power should be high enough to obtain sufficient signal to noise ratio, but low enough to avoid nonlinearities due to saturation. The saturation power $P_0 = V_0 \cdot 2R_0$ where R_0 is the resistance value on the bias point and V_0 is the voltage across the TES. Assuming a normal TES resistance of $R_N = 100$ mΩ and a bias point of 40 % of the superconducting to normal transition R_0 is equal to 40 mΩ. The voltage across the TES is calculated from the relation NEP= $V_0 * \sqrt{S_I}$ with $\sqrt{S_I}$ is the current to noise responsivity and NEP=$2 \cdot 10^{-19}$ W/$\sqrt{Hz}$. The TES noise is 16 pA/$\sqrt{Hz}$ in the electro thermal feedback (ETF) bandwidth. The voltage across the TES is equal to 12.5 nV and the saturation power is 4 fW. The signal source power chosen for beam measurements is 50% of the saturation power.

To correct for drift and 1/f noise, the signal is modulated, either by a dedicated chopper or by the instrument FTS mechanism movement. The signal to noise ratio S/N is required to be 1000. From this value the integration time is calculated: The noise N is 2π NEP/$\sqrt{0.5\tau}$ where 2π is the crest factor, $1/\tau$ is the bandwidth and the factor 0.5 comes from the chopper duty cycle. With a signal power of 2 fW per pixel a S/N of 1000 is reachable with 1 s of integration time. This enables "on the fly" scans rather than step and integrate, which would lead to unwanted vibrations and dissipation in the system.

The pinhole size can be calculated from the convolution between the Airy function and a box car function corresponding to a pinhole disk (see Fig. 2).
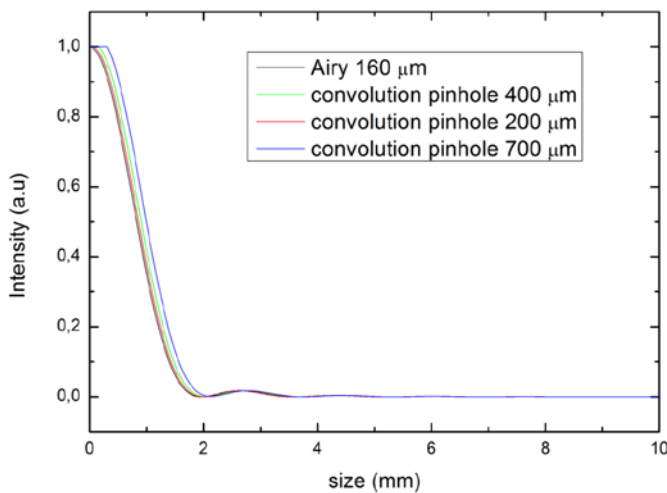

Fig. 2. Convolution of the Airy disk and a pinhole of different sizes for LW band.

The optimum pinhole diameters are 109, 198 and 372 µm for the SW, MW and LW bands respectively. The Airy disk will be oversampled (about 150 samples) to measure the FHWM and the Airy rings position within an accuracy of 5%. The scan speed is determined by the integration time and the allowed spatial smearing due to on the fly integration. The planned speed is one pinhole radius per second, corresponding to 50 µm/s for the SW band. The required relative accuracy of

the pinhole position with respect to the SAFARI FPU beam is 10 µm for the SW band.

For the beam direction and focal plane geometry scans a back-illuminated mask is used rather than a single pinhole, to shorten the test duration. The size of the mask is 20 x 20 mm, similar to the focal plane size. The distance between two pinholes on the same mask is determined from the Airy disk size and the expected cross-talk levels

The stray light test in the object focal plane is performed with a single pinhole rather than a mask, to ensure that a stray light path can be uniquely determined. Since this pinhole for stray light tests needs to move out of the object focal plane by 20 mm on all sides, the travel for the scanner is 60mm x 60 mm.

D. Calibration source

For the radiometry tests of SAFARI a calibration source is designed. It is coupled to the instrument via the reimager and a flip mirror in the OGSE optical path, see Fig. 1. The output port of the calibration source is positioned in the reimaged focal plane. The calibration source must offer a homogeneous field over the entire reimaged focal plane with well-known frequency and power. Homogeneous illumination can be achieved by making use of an integrating sphere with an output port diameter at least 5 times smaller than the sphere diameter, in order to produce sufficient reflections inside before the light escapes. In order to keep the spectrum of the input signal unperturbed, the reflectivity of the inner surface must be close to 99% and the sphere needs to be cooled to 1.7K.

To obtain the required spectrum as well as a stable output power a black body is used with a temperature of around 100K. The black body consists of a spherical cavity coated on the inside with black absorber. It has a small opening, thus approaching a perfectly black cavity.
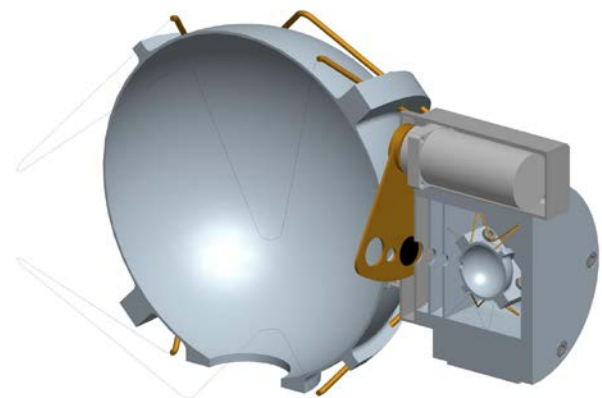

Fig. 3. Calibration source conceptual design.

The power level is reduced by a factor 10^6 to match SAFARI's operational range of 10^{-19} to 10^{-14} W per pixel. This reduction is achieved by geometric dilution: The coupling between the black body and the input of the integrating sphere is determined via the sizes of the two ports and their separation,

see Fig. 3. This determines the fraction of the solid angle π from the output of the black body that is coupled to integrating sphere. The remaining power is absorbed in the baffles, requiring a high absorption of the absorbing coatings on these baffles. A mechanism on the input port of the integrating sphere allows the choice of various opening diameters, expanding the power range in steps without altering the spectrum. By fast opening and closing the source can be used as a flasher. Optionally a frequency selective element like an etalon can be inserted to create well known spectral features.

The loading per pixel of the SAFARI instrument can be calculated as a function of the black body temperature. Fig. 4 plots these values for the three detector bands.
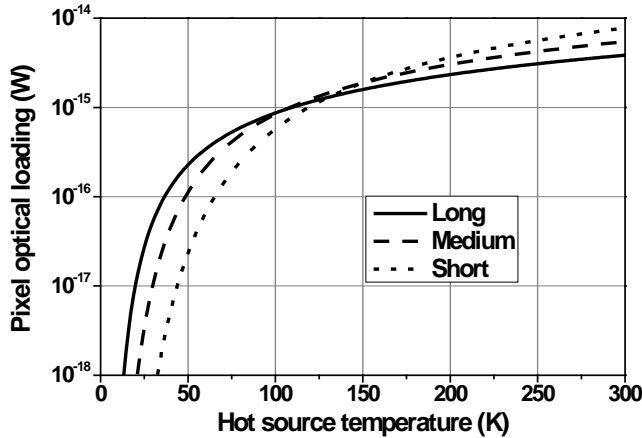

Fig. 4. Pixel loading versus black body temperature.

IV. STRAY-LIGHT CONTROL

The requirement on the background power level in the 4K compartment of the test cryostat is specified as the radiance level at the focal plane causing an increase in the SAFARI NEP of less than 20%. In order to reach this level, a combination of light tightness and stray light control measures is taken and a limit on the maximum temperatures inside the 4K OGSE space is set.

A. Absorber area

To model the effect of absorber in the 4K compartment, the test cryostat is treated as an integrating sphere which is coupled to the instrument via the pupil stop. The input signal is a hot source, e.g. the scanner actuator with a certain surface area, emissivity and temperature and corresponding IR power. If the sphere would be perfectly reflective all power from the source will make it to the exit port and from there will couple to the detector. Therefore a low-background environment requires absorbers in the OGSE compartment. Fig. 5 shows the loading of the TES pixels as a function of the fractional absorbing area. For the model a 1 meter diameter cryostat is used with emissivity 0.01. The absorber is modeled to have an emissivity of 0.99. Inside the cryostat the warm element is modeled by sphere of 40 mm diameter at a temperature of 20K and an emissivity of 0.1. The warm element is not in direct line of sight to the instrument.
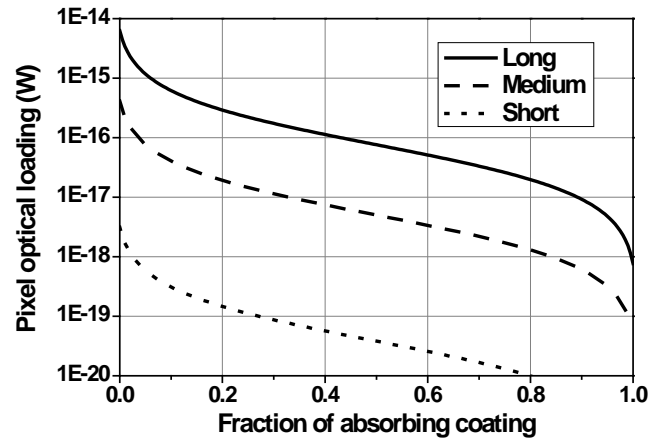

Fig. 5. Pixel loading versus fraction absorbing coating.

The attenuation versus fraction of absorbing coating is highly non-linear. The first 15% absorbing coverage of the 4K compartment wall already gives 10 dB of attenuation. The maximum temperature inside can be calculated as well: Assuming an absorbing coating fraction of 20% the NEP is increased by 20% for a 20mm diameter sphere with an emissivity of 0.1 and a temperature of 8K.

B. Light tightness measures

To ensure light from higher temperature shields does not reach the 4K compartment tongue and groove structures filled with carbon-loaded Stycast are used for mechanical connections that require regular mounting/demounting. The cable harness is led through Stycast filled meandering feedthroughs as well.

V. SUMMARY

The test setup of the SAFARI instrument is in a definition phase. Preliminary modeling has resulted in requirements for the calibration source and beam measurement equipment. The stray light control measures are being designed.

REFERENCES

[1] G.L. Pilbratt et al, "Herschel Space Observatory: An ESA facility for far-infrared and submillimetre astronomy", *Astronomy & Astrophysics*, vol. 518, July 2010, pp L1.
[2] M.J. Griffin et al, "The Herschel-SPIRE instrument and its in-flight performance", *Astronomy & Astrophysics*, vol. 518, July 2010, pp L3.
[3] P.D. Mauskopf et al, "Development of transition edge superconducting bolometers for the SAFARI Far-Infrared spectrometer on the SPICA space-borne telescope", in *Millimeter and Submillimeter detectors for astronomy IV* , SPIE 70200N (2008)
[4] R.S. Bhatia et al, "The effects of cryocooler microphonics, EMI, and temperature variations on bolometric detectors", *Cryogenics* vol 41, 2002 pp 851–863.
[5] G. Jacob et al, "Herschel –PACS Ground Calibration: the MPE Cryogenic Test Facility", *Astronomical Telescopes and Instrumentation*, SPIE 5487-106 (2004)
[6] T. Belenguer et al, "MIRI Telescope Simulator", SPIE 7010-39 (2008)